Battery Safety Testing with Accelerating Rate Calorimetry (ARC): Thermal modeling for adiabatic optimization, and kinetics-based validation

Finn van Ginneken[1,2*], Philipp Menke[2], Wilhelm Tegethoff[1,2]

[1] *TLK-Thermo GmbH, Rebenring 31, 38106 Braunschweig*
[2] *Institut für Thermodynamik, Technische Universität Braunschweig, Hans-Sommer-Straße 5, 38106 Braunschweig*
[3] *Physikalisch-Technische Bundesanstalt Bundesallee 100, 38116 Braunschweig*
[*]f.van-ginneken@tlk-thermo.com

Abstract

Accelerating rate calorimetry (ARC) is a fundamental experimental method for characterizing the thermal runaway (TR) behavior and reaction kinetics of lithium-ion batteries [1, 2]. Accurate extraction of kinetic parameters, however, requires an in-depth understanding of the internal and external heat transfer mechanisms governing the calorimeter and its containment vessel (canister). In conventional data evaluation, parasitic heat losses and thermal inertia are typically accounted for using a static thermal-inertia (Φ-factor) correction. This approach assumes idealized adiabatic conditions and uniform temperatures, which systematically underestimate self-heating rates, mask the true onset of TR, and obscure the experimental uncertainty in canister setups [2, 3]. To overcome these limitations and systematically assess the associated measurement uncertainties, this contribution presents two complementary approaches: First, a physics-based, lumped-parameter thermal network model of the ARC-canister system, developed in Modelica, resolves the dominant conduction, convection, contact, and radiation heat paths between six coupled thermal capacities representing the chamber walls, canister, clamping plates, and sample. Fitted against the cooling phases of two independent experiments, the model reproduces the transient temperatures with high accuracy ($R^2 > 0.999$) over the entire duration of the experiment. Second, an electrically driven, closed-loop kinetics emulator reproduces the decomposition of di-tert-butyl peroxide (DTBP) as a real, temperature-coupled heat source inside the same calorimeter, testing whether a chemically well-characterized exotherm remains detectable once realistic parasitic losses are present. Together, both approaches establish the foundation for a dynamic, physically grounded correction of measured self-heating rates for real battery cells, extending the classical static thermal-inertia (Φ-factor) correction.

1 Motivation

For more than four decades, the ARC has served as the standard instrument for adiabatic testing of thermal hazards and TR, ranging from traditional chemical process safety to modern lithium-ion battery cells [4]. The interpretation of ARC data relies on the assumption that the heat generated by a decomposing or self-heating sample is either retained within the sample and its container or can be corrected in a precisely defined manner. However, practical challenges complicate this evaluation. For instance, if an uncontrolled pressure release occurs and the ARC vents through its lid – as observed during preliminary tests – adiabaticity is lost. While using a pressure vessel (canister) can eliminate this leakage path, it introduces a new, non-negligible heat dissipation pathway around the sample. Recent literature confirms that such heat transfer limitations represent a major, frequently overlooked cause for the underestimation of reaction rates in ARC tests [2]. Furthermore, specialized correction methods based on explicit heat transfer models are essential to accurately interpret such data [3].

The present work is embedded in the *TransMeT* project [5], which investigates how the aging of lithium-ion batteries affects their TR behavior and thermal safety margins compared to pristine battery cells. The methodology presented here, developed for an ARC test on battery cells conducted inside a pressure-tight canister – in which preliminary tests showed that cells failed to reach TR – provides a basis for the necessary specialized correction methods.

2 Thermal Network Model of the ARC-Canister System

To quantify parasitic heat losses, a lumped-parameter thermal network model of the full assembly was developed in Modelica (Fig. 1). The model represents the canister lid, shell, and base as geometry-based thermal capacities derived from their steel volume, and the two clamping plates together with the sample between them as mass-based capacities. The three ARC chamber-wall temperatures (top, side, bottom) are defined as measured boundary conditions. The sample itself carries no internal heat source in this configuration, so the model isolates the parasitic heat loss network from any actual cell chemistry.

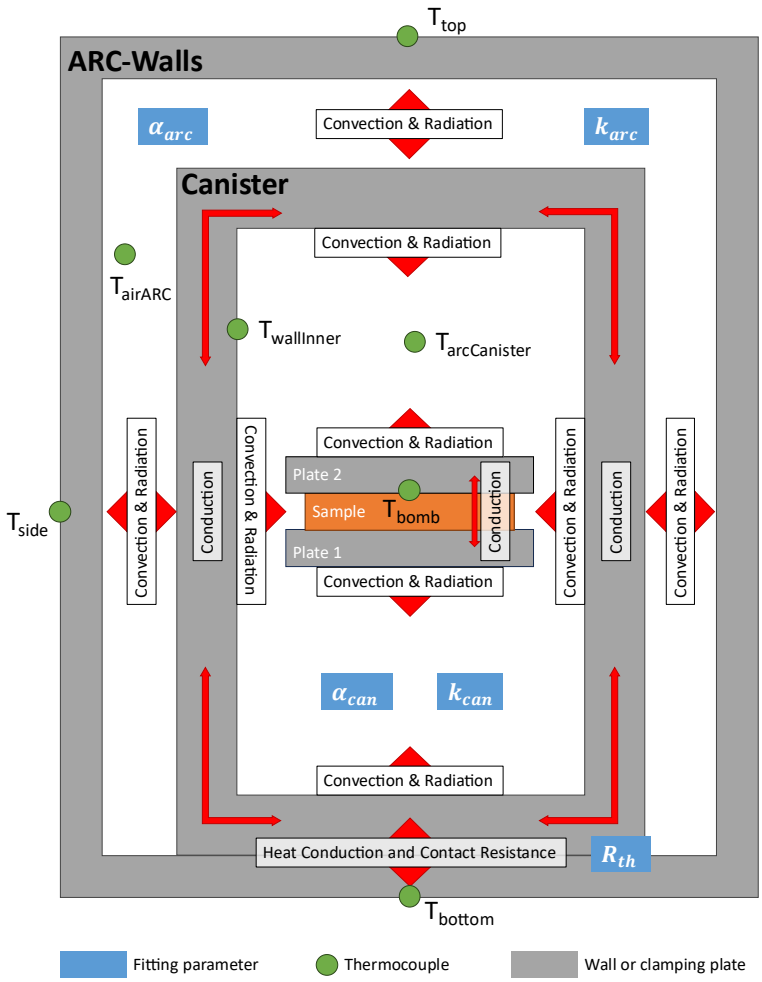

Fig. 1: Thermal network of the ARC-canister-sample system. Blue boxes mark the five fitting parameters of the model; green markers denote the thermocouple locations, of which T_{side}, T_{bottom}, and T_{top} serve as measured boundary conditions.

For every node j (canister wall segments, canister air, clamping plates, sample), the model integrates the heat balance equation in which the conductive $\dot{Q}_{\mathrm{cond}}$, convective $\dot{Q}_{\mathrm{conv}}$ and radiative $\dot{Q}_{\mathrm{rad}}$ paths of Fig. 1 enter separately:

$$m_j c_{\mathrm{p},j} \cdot \frac{dT_j}{dt} = \dot{Q}_{\mathrm{cond},j} + \dot{Q}_{\mathrm{conv},j} + \dot{Q}_{\mathrm{rad},j} + \dot{Q}_{\mathrm{heater},j} \tag{2.1}$$

with node-specific heat capacity $c_{\mathrm{p},j}$ and mass m_j. The source term $\dot{Q}_{\mathrm{heater},j}$ is zero everywhere except at the sample node, where it accepts the electrically emulated heat release of Section 3. The convective contributions carry the two gap coefficients of Fig. 1: α_{arc} for the gap between the ARC chamber walls and the outer canister surfaces, α_{can} for the gap between the canister cavity and the clamping plates.

$$\dot{Q}_{\mathrm{conv,arc\to can},j} = \alpha_{\mathrm{arc}} A_{\mathrm{j}} (T_{\mathrm{arc},j} - T_{\mathrm{can},j}) \tag{2.2}$$

$$\dot{Q}_{\mathrm{conv,can\rightarrow plate},j} = \alpha_{\mathrm{can}} A_j (T_{\mathrm{can},j} - T_{\mathrm{plate},j}) \tag{2.3}$$

The conductive path from the canister base to the ARC chamber floor is modeled as a series of wall conduction and mechanical contact, represented by the specific contact resistance R_{th} shown in Fig. 1.

$$\dot{Q}_{\mathrm{cond,bottom}} = \frac{A_{\mathrm{contact}}}{R_{\mathrm{th}}} \left(T_{\mathrm{bottom}} - T_{\mathrm{can,bottom}}\right) \tag{2.4}$$

Radiation is not modelled as a sum of pairwise surface-to-surface exchange. Instead, each of the two cavities, the outer one between the ARC walls and canister and the inner one between canister walls and clamping plates, is treated as a closed grey-body enclosure in which every participating surface j exchanges heat with a single virtual grey surface representing all remaining surfaces of that enclosure [6]:

$$\dot{Q}_{\mathrm{rad},j} = k Gr_j \sigma (T_j^4 - T_{\mathrm{virt},j}^4), \quad Gr_j = \frac{A_j}{\frac{1}{\epsilon_j} + \frac{1}{\epsilon_{\mathrm{virt,j}}} - 1} \tag{2.5}$$

$$\text{with } k = k_{\mathrm{arc}} \text{ for the outer and } k = k_{\mathrm{can}} \text{ for the inner enclosure}$$

$$T_{\mathrm{virt},j} = \frac{\sum_i A_i T_i - A_j T_j}{\sum_i A_i - A_j}, \quad \epsilon_{\mathrm{virt},j} = \frac{\sum_i A_i \epsilon_i - A_j \epsilon_j}{\sum_i A_i - A_j} \tag{2.6}$$

Here σ is the Stefan-Boltzmann constant, and k_{arc} and k_{can} are the two multiplicative radiation fit factors from Fig. 1. Since the virtual surface temperature T_{virt} is calculated as the area-weighted average of the remaining surface temperatures and not as the average of their fourth powers, the individual surface currents do not add up exactly to zero. The residual amount is therefore redistributed in proportion to the areas, ensuring that no energy is lost. Of five parameters appearing in Equations (2.2)-(2.6) the two gap coefficients ($\alpha_{\mathrm{arc}}, \alpha_{\mathrm{can}}$) and the outer radiation factor (k_{arc}) are identified from cooling phases of the data in the following section together with the clamping-plate mass and heat capacity, while the inner radiation factor (k_{can}) and the base contact resistance (R_{th}) remain open. The overall structure extends the classical Townsend-Tou framework for adiabatic calorimeters and thermal-inertia (Φ-factor) correction [7] from a single lumped mass to a partly resolved, geometry-based multi-node network.

2.1 Parameter Identification and Fit Quality

Because convective and radiative heat paths can partially compensate for one another, two trials are fitted jointly rather than in isolation, in a single nonlinear least-squares problem. The Modelica model is simulated directly from its source code via the Dymola Python API, driven by the three measured chamber-wall temperatures for each trial. The model strictly receives these three boundary temperatures as inputs, while the heater power is set to zero; the sample temperature is obtained as the model output. For every trial and fit target, the residual (simulated minus measured) is scaled by the square root of a per-trial and per-target weight divided by the number of evaluated sample points. This normalization ensures that neither a finer logging raster nor an additional trial disproportionately dominate the objective function. A failed simulation is assigned a fixed residual penalty rather than aborting the optimization run.

The concatenated residual vector across both trials is minimized using SciPy's *least_squares* solver (trust region reflective algorithm, method *trf*). Parameters spanning several orders of magnitude are optimized in a logarithmic space, with a finite-difference step deliberately set above the numerical noise.

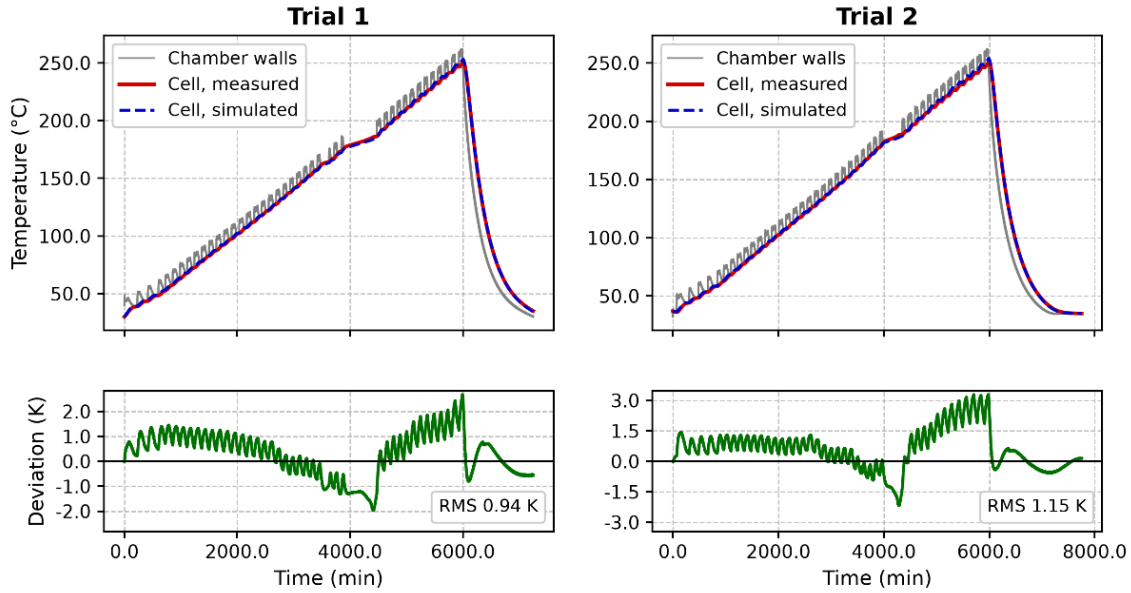

Fig. 2: Measured vs. simulated sample temperature and residuals for the two cooling-phase fit trials used to identify the thermal network parameters

Three heat transfer coefficients were identified jointly on the cooling phases: the chamber-canister gap coefficient ($\alpha_{\mathrm{arc}} \approx 4.52\ \mathrm{Wm^{-2}K^{-1}}$), the canister-plate gap coefficient ($\alpha_{\mathrm{can}} \approx 4.50\ \mathrm{Wm^{-2}K^{-1}}$), and the outer radiation correction factor (k_{arc}), which converged towards zero. Masses, heat capacities, and geometry enter as measured inputs and were not fitted. Within the fit windows the model reproduces the sample temperature with a root-mean-square deviation of 0.61 K and 0.45 K. Keeping these parameters unchanged, a second, independent pass re-simulates each trial completely: over cycles of 121 h and 129 h, including heat-wait-seek ramps, the model follows the measured sample temperature to 0.94 K and 1.15 K RMS (R^2 = 0.9998 and 0.9997). The Jacobian matrix of the fit illustrates that the gap coefficients are strongly negatively correlated (r = −0.98). Thus, the data determines the total resistance between the sample and the chamber, rather than its distribution across the two gaps. Nevertheless, the model structure from Section 2 can describe the thermal behavior of the ARC canister over the entire temperature range and serves as a suitable basis for quantifying its parasitic losses.

3 Kinetic simulation of a known decomposition reaction

The previous section explained that the network model can describe how heat flows into or out of the sample location. Another crucial question when testing a battery is: can reaction kinetics be recovered from the ARC measurement, and by how much must it be corrected to match the kinetics that took place? For a real sample, this question cannot be answered directly because the measurement itself is the only source of kinetics. There is no independent reference to compare the evaluated Arrhenius parameters against.

The hardware-in-the-loop approach inverts this situation. The kinetics is prescribed, so its parameters - activation energy (E_{a}), frequency factor (A), reaction order (n), and mass-specific reaction enthalpy ($\Delta_{\mathrm{R}}h$) - are known exactly beforehand. Evaluating the resulting measurement with the usual ARC procedure and comparing the recovered parameters with the prescribed ones therefore yields a direct measure of the systematic error introduced by the apparatus, providing a basis on which a correction can be derived and verified.

Di-tert-butyl peroxide (DTBP) in toluene is used as the prescribed reaction because it is the established benchmark substance for adiabatic calorimeters and its kinetics is well documented. Reproducing it electrically rather than chemically avoids the usual experimental uncertainties of weighing, partial evaporation, or impurities. The reaction is directly computed analytically from literature kinetics (Section 3.1) and then physically reproduced inside the calorimeter as an electrical heat source (Section 3.2).

3.1 Analytical reaction kinetics

The reaction progress of the DTBP decomposition is governed by an n-th order Arrhenius rate law,

$$\frac{d\alpha}{dt} = k \cdot (1-\alpha)^n = A \cdot \exp\left(-\frac{E_\mathrm{a}}{RT}\right) \cdot (1-\alpha)^n, \quad \text{with } n = 1 \text{ for DTBP/toluene} \tag{3.1}$$

With α as degree of conversion, k as rate constant, E_a as activation energy, A as frequency factor, T as temperature, and R as the ideal gas constant. Rather than integrating this equation with an explicit method, such as Euler's method, which becomes numerically unstable once $k\Delta t$ exceeds one, a condition already reached at moderate temperatures, the emulator integrates the rate law in closed analytical form. To account for the temperature rise during this interval $[t, t+\Delta t]$, it uses the trapezoidal average of the rate constant, $\bar{k}$:

$$\bar{k} = \frac{1}{2}[k(T_t) + k(T_{t+\Delta t})] \tag{3.2}$$

$$\alpha_{t+\Delta\mathrm{t}} = \begin{cases} 1 - (1-\alpha_t) \cdot \exp\left(-\bar{k}\Delta t\right), & n = 1 \\ 1 - \left[(1-\alpha_t)^{1-n} + (n-1)\bar{k}\Delta t\right]^{\frac{1}{1-n}}, & n \neq 1 \end{cases} \tag{3.3}$$

This closed-form solution is exact for arbitrary step size, cannot overshoot $\alpha = 1$, and is combined with an interval-averaged reaction rate $d\alpha(dt)^{-1} = \Delta\alpha(\Delta t)^{-1}$ so that the delivered electrical energy exactly matches the chemical heat release. The kinetic parameters used in this work ($E_\mathrm{a} = 156.3$ kJ mol^{-1}, $\log(A) = 15.7$, $\Delta_\mathrm{R}h = 284.2$ J g^{-1}) were taken from literature for the same 20 wt% DTBP in toluene mixture [8], for which DSC characterization reports an onset temperature of 155.1 °C and a peak temperature of 181.5 °C.

3.2 Hardware-in-the-loop realization

To reproduce these kinetics as a real temperature-coupled heat source inside the ARC, a closed-loop emulator receives the ARC's temperature signal ($\Delta t \approx 6$ s) and converts the reaction rate of Equation (3.3) into an electrical heater power

$$P(t) = m_\mathrm{DTBP}\Delta_\mathrm{R}h\frac{\Delta\alpha}{\Delta t} \tag{3.4}$$

delivered to a heating foil clamped between two aluminum plates with a thermal pad inside the canister. This heater fixture is mechanically analogous to, but not identical with, the clamping-plate pair of Section 2. Because this setup uses different plates and altered thermal masses, the parameter set identified in Section 2 cannot be directly transferred. The required electrical power is calculated based on the DTBP mass and the enthalpy of decomposition and is independent of the mounting; what the mounting does affect is the temperature behavior at this power level. This change in temperature behavior would need to be determined through a separate test for this configuration. This missing information, however, limits only the predictions of the emulator's temperature trace, but not the validity of the emulation itself. Following the Joule-heating approach recently proposed for ARC performance evaluation [9], the reaction is driven by the ARC's own measured temperature signal, so the delivered power responds to the true, loss-affected sample temperature rather than following a pre-computed adiabatic schedule. The parasitic losses of the system thus enter the emulated exotherm inherently without having to be modelled beforehand.

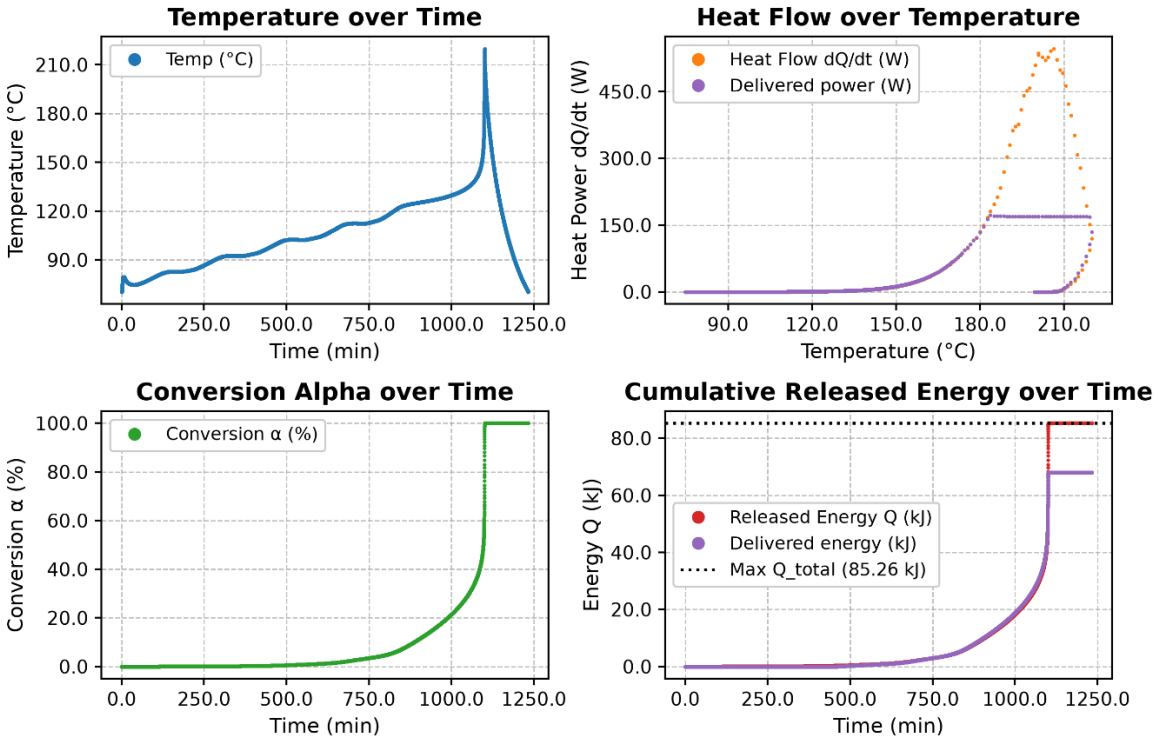

Fig. 3 (preliminary): Hardware-in-the-loop emulation of the DTBP/toluene (20 wt%) decomposition: sample temperature vs. time, heat-release rate vs. temperature, conversion vs. temperature, and cumulative released energy vs. time.

Initial experiments of this kind show the expected Arrhenius-like increase in the heat release rate with rising temperature (Fig. 3). In adiabatic calorimeters, a deviation from ideal Arrhenius behavior is known to occur above a critical self-heating rate; in the present pressure vessel setup, such deviations are also to be expected at high rates. Heat conduction losses through metallic mounting and assembly elements as well as the thermal inertia of the pressure vessel are expected to influence the measured self-heating rate.

As visible in the heat-flow and energy profiles of Fig. 3, the emulated power saturates at approximately 170 W above 185 °C due to the electrical current and voltage limits of the power supply. Dimensioning the virtual reactive mass m_{DTBP} represents a critical trade-off: it must be chosen large enough to generate an unambiguous, detectable self-heating onset and a substantial adiabatic temperature rise against the canister's parasitic heat losses, as well as small enough to keep the peak reaction power within the safe operating envelope of the heater and electrical source.

Since the thermal network model (Section 2) explicitly maps the conduction and convection pathways, it should be able to physically reproduce these deviations rather than merely capture them phenomenologically. A prerequisite for this is the recharacterization of the existing heater configuration and the subsequent coupling of both modules (Section 4). A future ARC experiment using a real sample cell (20 wt% DTBP in toluene) will serve to experimentally validate the hardware-emulated curve.

4 Conclusion and Outlook

In summary, the thermal network model and the experimental heating device provide the methodological basis for combining real and emulated heat flows via a defined boundary condition at the sample node. As an immediate follow-up, the combined application of both subsystems is planned. Because the current heating fixture (Section 3.2) differs slightly from the passive test setup in terms of thermal mass, a dedicated parameter identification run will first be performed for this specific configuration.

The subsequent investigation consists of two main steps:

- **Model validation under active heating:** Using the DTBP baseline, the thermal network will be verified under dynamic heating loads, enabling a refined calibration of temperature-dependent radiation losses and contact resistances at elevated temperatures.
- **Dynamic loss correction for real TR tests:** In reverse operation, the validated network will serve as a physical observer to reconstruct the unperturbed reaction rates from real battery runaway data. Instead of relying on blanket thermal-inertia (Φ-factor) corrections, this approach achieves a true decoupling of cell decomposition kinetics from the surrounding calorimeter and canister environment.

This methodology provides an essential framework within the *TransMeT* project [5] to define experimental limits a priori and evaluate the true impact of battery cell aging on an apparatus-corrected basis.

5 References

[1] X. Feng, D. Ren, X. He, and M. Ouyang, "Mitigating Thermal Runaway of Lithium-Ion Batteries," *Joule*, vol. 4, no. 4, pp. 743–770, 2020, doi: 10.1016/j.joule.2020.02.010.

[2] S. Dutta, K. A. Mulligan, B. L. Drake, K. L. Simmons, A. L. Koziol, and S. E. Horsch, "Is your ARC data misleading? Heat-transfer limitations and reaction rate underestimation in Accelerating Rate Calorimetry," *Process Safety and Environmental Protection*, vol. 168, pp. 1212–1218, 2022, doi: 10.1016/j.psep.2022.10.022.

[3] D. Chen *et al.,* "Heat dissipation analysis and correction of the sample in accelerating rate calorimetric experiment," *Thermochimica Acta*, vol. 733, p. 179695, 2024, doi: 10.1016/j.tca.2024.179695.

[4] J. Ding *et al.,* "Accelerating rate calorimetry: History, state of the art and perspectives," *Chemical Thermodynamics and Thermal Analysis*, vol. 18, p. 100182, 2025, doi: 10.1016/j.ctta.2025.100182.

[5] I. Frischmuth. "PTB und eine Industriepartnerin forschen für den sicheren Einsatz gealterter Batterien: TransMeT." Accessed: Sep. 14, 2026. [Online]. Available: https://www.ptb.de/cms/presseaktuelles/journalisten/nachrichten-presseinformationen/presseinfo.html?tx_news_pi1%5Bnews%5D=15027&tx_news_pi1%5Bcontroller%5D=News&tx_news_pi1%5Baction%5D=detail&tx_news_pi1%5Bday%5D=21&tx_news_pi1%5Bmonth%5D=10&tx_news_pi1%5Byear%5D=2025&cHash=d917dbe28dab45309fbc4b87b95d8025

[6] C. Kaiser, "Untersuchungen zur Effizienz- und Leistungssteigerung von Omnibusklimaanlagen," Universitätsbibliothek Braunschweig, 2020.

[7] D. I. Townsend and J. C. Tou, "Thermal hazard evaluation by an accelerating rate calorimeter," *Thermochimica Acta*, vol. 37, no. 1, pp. 1–30, 1980, doi: 10.1016/0040-6031(80)85001-5.

[8] Q. He *et al.,* "Comprehensive study on thermal hazards and chemical kinetics of thermal decomposition of di-tert-butyl peroxide," *Thermochimica Acta*, vol. 752, p. 180092, 2025, doi: 10.1016/j.tca.2025.180092.

[9] W. Liang *et al.,* "Performance evaluation approach for accelerating rate calorimeters by means of Joule heat," *Thermochimica Acta*, vol. 735, p. 179719, 2024, doi: 10.1016/j.tca.2024.179719.